

Quantum reservoir networks based on decoherence-free subspaces

V.V. Akshay

*School of Nanoscience and Nanotechnology, Mahatma Gandhi University,
Priyadarsini Hills, Kottayam, Kerala, 686560, India**

M.V. Altaisky

Space Research Institute RAS, Profsoyuznaya 84/32, Moscow, 117997, Russia[†]

N.E. Kaputkina

National University of Science and Technology 'MISIS', Moscow, 119049, Russia[‡]

We present numerical simulation of a six-qubit quantum reservoir network with an output implemented on a 5-dimensional decoherence-free subspace (DFS), working as a classifier between entangled and product states of the input quantum system, fed to the reservoir during a finite learning time. Since the dynamics of DFS is not affected by external fluctuations, no cooling is required, and the proposed model seems a promising candidate for future quantum artificial intelligence systems working at room temperatures and free of huge energy consumption.

I. INTRODUCTION

Quantum computing (QC) and artificial intelligence (AI) are two of the most flourishing branches of modern computer science. Both have deserved their credibility due to the essential parallelism of data processing, which enables them to outperform classical computational methods, and both share the same bottleneck of a huge energy consumption. This obstacle makes the creation of commercially effective AI systems of superhuman level [1] extremely problematic, if not impossible.

At the beginning of the quantum computational era, when Deutch proposed a circuit-based quantum computer [2], the main attention was paid to the computational efficiency of quantum algorithms. In this way, the Shor algorithm, being based on quantum fast Fourier transform, can solve exponentially hard factorisation problems in polynomial time due to the inherent quantum parallelism of information processing [3]. For the same reason, the Grover database search algorithm finds an unknown record in a database by \sqrt{n} steps only, instead of $n/2$ steps of a classical search [4].

The main practical problem for algorithmic circuit-based quantum computers remains to keep many qubits of a quantum data processing unit in a state of quantum superposition, which provides the quantum parallelism of data processing. The quantum superposition states are rather fragile and can be destroyed by merely small fluctuations of the environment. This is the *decoherence problem* [5, 6]. For the reason of decoherence, most of the present quantum data processing systems operate at very low temperatures, less than 1°K. Those are SQUIDs, ions in traps, and quantum dots – maybe all except optical systems.

Low operation temperature implies an expensive cooling system and prohibits scalable technology, which we wish for portable devices. The main remedy for errors in computation caused by decoherence is the quantum error correcting codes (QECC), implemented by a system of quantum gates, which can correct the erroneous qubits based on the redundant data processed by a given algorithm [7, 8].

Surprisingly, the initial idea of quantum computers, as first proposed by R. Feynman [9], was not algorithmic at all – it was a simulation of the physical system of interest by a *smaller* quantum system – a direct simulation. The modern AI systems, which keep burning gigawatts of energy on classical hardware, are waiting for a future energy-effective implementation and are non-algorithmic by their nature – They are based on neural networks. The idea of a neural network (NN) is a mathematical endeavour to describe the work of the brain, first formulated by Hebb [10]. In a general sense, a neural network is a massively parallel distributed processor made up of simple processing units [neurons] that has a natural propensity for storing experiential knowledge [in interneuron connections] and making it available for use [11]. In the case of a hardware implementation of *artificial* neural network (ANN), the change of weights – connections between neurons – during the learning process is performed by *learning algorithms*, implemented on classical computational hardware. In a physical or biological implementation, there is no prescribed algorithm: the neural network operates as a simulator, obeying the laws of physics.

The reason for tremendous effectiveness of the human brain in comparison to numerical computer algorithms may be not only the inherent parallelism of neural networks (which is also a case for modern deep-learning systems [12]), but also the quantum nature of data processing. The idea that the human brain is a kind of quantum computer was put forward by different authors [13–17]. The main argument that precludes the scientific com-

* vvakshay285@gmail.com

† altaisky@cosmos.ru

‡ kaputkina.ne@isis.ru

munity from taking this idea seriously was the Tegmark estimation of decoherence time for biomolecular systems to be about $\tau_{\text{decoh}} \propto 10^{-19} \div 10^{-13} \text{s}$, from ions to microtubules, respectively [18].

At the same time, we have to admit that the biological brain somehow escapes the thermodynamic limit of heat dissipation $\Delta Q \geq k_B T \ln 2$ per operation; otherwise, it would be boiled out, which never happens. This argument may be a hint that *in vivo* neural networks somehow escape simplistic Tegmark's consideration and may keep quantum coherence for a long time at room temperature without any external cooling system [19].

A mathematical model for avoiding dissipation has been proposed by several authors in the context of quantum computers [20, 21]. It is based on symmetry considerations of the system-environment interaction and consists of coding the information in decoherence-free subspaces (DFS)[20]. DFS has been actively discussed in the context of circuit-based quantum computers but was first proposed for application in quantum neural networks in [22].

In the present paper, we consider a model of a six-qubit reservoir-type quantum neural network, the output of which is formed by the projections of the six-qubit reservoir network state onto a 5-dimensional DFS. The dimension 5 turns out to be sufficient for fairly good classification of both two-qubit input states and squeezed input states in the Fock basis in two classes of entangled and product states, respectively.

The remainder of this paper is organized as follows. In *Sec. II* we recall the ideas of DFS, as was proposed in [20]. In *Sec. III* we outline the model of quantum reservoir network used for quantum data classification. *Sec. IV* presents the dynamics of the quantum reservoir network used for the classification of input quantum states into entangled and product classes. The simulations are presented in the Lindblad approximation for two different types of input states: (A) two-qubit teacher states; (B) two-mode squeezed teacher states. In *conclusion*, we summarize the results and discuss the open problems of our approach.

II. DECOHERENCE-FREE SUBSPACES

The dynamics of any quantum information processing system (whatever it may be, a circuit-based computer, quantum neural network, or anything else) embedded into a noisy environment can be described by a Hamiltonian of the form

$$H = H_S + H_B + H_I, \quad (1)$$

where H_S is the Hamiltonian of the processing system itself, H_B is the Hamiltonian of the environment, and H_I is the Hamiltonian describing the interaction between the system and its environment.

The combined system (data processing unit and its environment) is a closed quantum system, and its quan-

tum evolution should be unitary. However, we cannot be aware of all the details of the environment dynamics and have to average over the states of the environment using the theory of open quantum systems (OQS) [23], i.e., we have to trace out the environment degrees of freedom to obtain the density matrix of the processing system itself.

In brief, the environment (B) works on the system (S) as a measuring device, which results in the decoherence – decay of the off-diagonal terms of the system density matrix ρ_S [24]. The principal role in the decoherence effects (or their absence) is played by the system-environment interaction Hamiltonian H_I , or, more precisely, by its symmetries.

Suppose a quantum register is represented by a usual register of N spin-bosons [25] described by a Hamiltonian

$$H_S = \epsilon \sum_{i=1}^N \sigma_i^z, \quad (2)$$

where σ_i^z is the Pauli matrix acting on the i -th qubit, and the environment is represented by a heat bath of harmonic oscillators, described by the Hamiltonian

$$H_B = \sum_k \omega_k b_k^\dagger b_k, \quad (3)$$

with the sum taken over all oscillator modes.

In the first-order approximation, the interaction Hamiltonian H_I describes spin flips in the system register caused by the absorption/emission of oscillator modes from/to the heat bath:

$$H_I = \sum_{i=1}^N \sum_k g_{ki} \sigma_i^+ b_k + f_{ki} \sigma_i^- b_k^\dagger + h_{ki} \sigma_i^z b_k + h.c., \quad (4)$$

where σ_i^α is the Pauli matrix acting on the i -th qubit.

If the coupling constants g_{ki}, f_{ki}, h_{ki} do not depend on the qubit number i , one can sum up over all qubits and construct the full Hamiltonian, describing the interaction of the whole register with the heat bath:

$$H_I = \sum_k g_k S^+ b_k + f_k S^- b_k^\dagger + h_k S^z b_k + h.c., \quad (5)$$

$$\text{where } S^\alpha = \sum_{i=1}^N \sigma_i^\alpha, \quad \alpha = \pm, z,$$

are the total spin operators of the qubit register.

The independence of coupling constants g_{ki}, f_{ki}, h_{ki} on the qubit number implies the wavelength of the environment oscillations is much bigger than the geometric size of the system S . This is known as the generalization of the Dicke limit in quantum optics [26].

Since each qubit in the register can be understood as a spin-one-half representation of $SU(2)$ group, i.e., it is described by a two-component spinor $\begin{pmatrix} \uparrow \\ \downarrow \end{pmatrix}$, for each *even*

value of N , the state of the whole register, which is the product of individual states, contains singlets. As it is known from group representation theory [27], the decomposition of a direct product of representations into a sum of representations

$$D_{\frac{1}{2}}^{\otimes N} = \sum_{j \in J} n_j D_j,$$

where each D_j is an irreducible representation of $SU(2)$ group, corresponding to the total angular momentum value j and having the dimension $(2j+1)$, with n_j being the number of times the representation D_j appears in the sum. For the $SU(2)$ group this gives the Clebsch-Gordan series:

$$\begin{aligned} D_{1/2} \otimes D_{1/2} &= D_1 \oplus D_0, \\ D_{1/2}^{\otimes 4} &= D_2 \oplus 3D_1 \oplus 2D_0, \\ D_{1/2}^{\otimes 6} &= D_3 \oplus 5D_2 \oplus 9D_1 \oplus 5D_0, \dots, \end{aligned} \quad (6)$$

and so on. Since the spin of a quantum state belonging to D_0 representation is zero, the action of the energy operator S^z on such a singlet state gives zero, and the actions of the ladder operators S^+ and S^- also give zero in total [20].

III. QUANTUM RESERVOIR PROCESSING

The presence of quantum superposition states is a key element that provides superiority of quantum computers over classical ones when solving a problem by means of quantum algorithms. For a wide class of problems, an *algorithmic* solution is not effective, even in the classical case. The example is image classification, where the task of the processor (either classical or quantum) is to assign to each input data vector an output vector, which labels the class. The dimension of input vectors is typically much higher than that of the output. A typical example is the classification between cats and dogs, where the input size is the total size of all pixels in the image, and the output size is one bit. For such non-algorithmic problems, we have to construct a mapping from a high-dimensional space of input data to a low-dimensional space of output classes. Since both the input and the output may be either classical (C) or quantum (Q), there may be four different types of data processing: CC, CQ, QC, QQ.

In case both the input and output data are classical, a universal function approximator, providing such a mapping, is a multilayer perceptron

$$y^{i+1} = f^{(i)}\left(\sum_k w_{ks}^{(i)} y_s^{(i)} + b_k^{(i)}\right), \quad (7)$$

where $f^{(i)}(\cdot)$ is a nonlinear neuron activation function on the i -th layer of the network. The inputs $y^{(i)}$ are fed to this function with a set of tunable weights and

biases $\{w_{ks}^{(i)}, b_k^{(i)}\}$, which are being optimized during the learning process. For a given learning set $\{y^{(0)}(s)\}_s$ with the known set of labels, $\{d(s)\}_s$ the learning consists in the optimization of weights and biases in a way that they minimize the average error $E(\omega, b) = \langle (y^{(N)}(s) - d(s))^2 \rangle_s$, or cost function, for some suitable measure on the training set [11].

The feed-forward networks, which are widely used in AI systems, form only one class of neural networks. In fact, any system comprised of identical units (neurons), generally with all-to-all connections, can be used as a neural network if we manage to optimize connection weights in a way that for all input vectors from the training set, its output is suitably close to the desired values.

Due to the linearity of quantum mechanics, there is no straightforward way to implement the *non-linear* activation function (7) in quantum settings and fed a linear combination of input states to it. It is, however, possible to harness quantum transitions and quantum tunnelling to drive the whole quantum system of interconnected qubits (neurons) of a data processing unit to a quantum state that minimizes a cost function and, therefore, provides a solution to a given optimization problem. This is the way commercial quantum annealers produced by D-Wave Systems Inc., implemented as Boltzmann machines on SQUIDS, operate [28].

In a classical artificial neural network with all-to-all connections the learning procedure requires tuning of $O(N^2)$ weights. This is computationally expensive. The idea of a *reservoir network* arose from recurrent neural networks [29, 30], and consists of tuning only the weights of the output layer. All other weights of a densely connected network – reservoir – are set to fixed random values at the beginning and play the role of a high-dimensional nonlinear kernel, which dramatically increases the capacities of the network, if compared to a linear model. Reservoir networks exist in both classical and quantum [29, 31] versions.

The operation flow chart of the reservoir network is schematically drawn in Fig. 1. The input data vector is fed to the reservoir – densely connected network with random weights. A small subset of the reservoir network, called the output layer, is connected to the system output by a set of tunable weights W_{ij}^{out} . Supervised learning process consists in tuning this very set of weights in order to minimize the learning error on the training set. Since the number of tunable weights is small, the learning process goes fast.

The generalization of reservoir network to the quantum case is straightforward [31], and specially attractive for the use of decoherence-free subspaces [22, 32].

IV. DATA CLASSIFICATION WITH QUANTUM RESERVOIR NETWORK

We have simulated the dynamics of six-qubit reservoir learning to distinguish between entangled and product

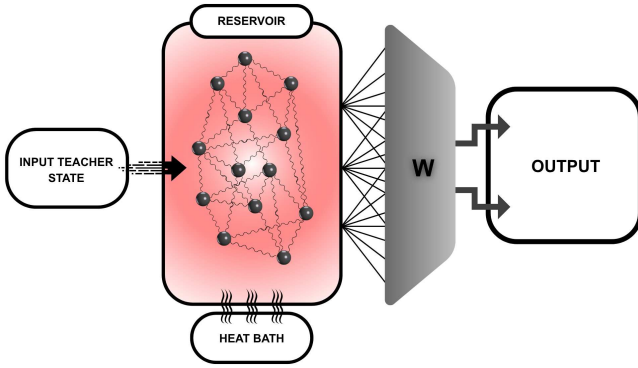


FIG. 1. Operation scheme of reservoir computing. A quantum input state is submitted to the input of a complex quantum system of identical particles, interacting with each other as a randomly connected network. This is called "reservoir". The reservoir incoherently interacts with its environment – heat bath. The quantum state at the output of the reservoir is filtered by a weight matrix W^{out} with tunable weights. The results of this filtering give output of the system. Redrawn from [31].

states fed to the input of the network. The reservoir is described by a Hamiltonian

$$H_R = \sum_{i,j=0}^5 J_{ij} (b_i^\dagger b_j + b_j^\dagger b_i), \quad (8)$$

where J_{ij} are random weights, homogeneously distributed in $[-1, 1]$ before the beginning of simulation, b_i^\dagger and b_i are the ladder operators of the i -th qubit in the reservoir.

The interaction between the reservoir qubits and the teacher quantum system is described by interaction Hamiltonian

$$H_I(t) = (1 - \theta(t - \tau)) \sum_{k=6}^7 \sum_{j=0}^5 f_k W_j (a_k^\dagger b_j + b_j^\dagger a_k), \quad (9)$$

where (a_k, a_k^\dagger) , $k = 6, 7$ are the ladder operators for the teacher, W_j are random input connection weights, f_k are the coupling constants of the teacher system, which we set to constant values, $\theta(\cdot)$ is the step function, which provides switching the interaction between the reservoir and the teacher on for a finite time τ .

At the initial instant of time, the quantum states of the teacher system and the reservoir are independent, and the density matrix ρ of the whole system [teacher+reservoir] is a direct product

$$\rho = \rho^{teach} \otimes \rho^{reservoir},$$

where $\rho^{reservoir}$ is the 64×64 density matrix of the reservoir qubits.

The evolution of the total density matrix ρ is given by the Lindblad-Gorini-Kossakowski-Sudarshan master

equation [31]:

$$i \frac{\partial \rho}{\partial t} = [H_R + H_I, \rho] + i \frac{\gamma}{2} \sum_j \mathcal{L}(b_j) + i \frac{P}{2} \sum_j \mathcal{L}(b_j^\dagger), \quad (10)$$

where H_R is the reservoir Hamiltonian (8). The interaction of reservoir with the fluctuating environment is described in Lindblad-Gorini-Kossakowski-Sudarshan approximation by the dissipation operator.

$$\mathcal{L}(x) := 2x\rho x^\dagger - x^\dagger x\rho - \rho x^\dagger x.$$

We assume that the pumping (P) and the dissipation (γ) are the same for all 6 qubits of the reservoir.

Before starting the learning process, we equilibrate the six-qubit reservoir density matrix $\rho^{reservoir}$, according to the same master equation (10), but in the absence of any teacher. The equilibration can be done either from a fixed [ground] state of the 6 qubit system, or from a random product state $\rho_*^{reservoir} = \otimes_{i=0}^5 \rho_i$, with ρ_i being random pure states of individual qubits. The equilibration of initial state of 6 qubit reservoir is shown in Fig. 2 below.

The task of the reservoir network is to classify the input states ρ^{teach} into two classes: the entangled and the separable states. Having submitted the input state ρ^{teach} to the reservoir, the state of the reservoir is changed due to its interaction with the teacher, given by H_I Hamiltonian (9), and the interaction with environment governed by master equation (10).

Having the interaction between the reservoir and the teacher during the time τ , at the instant of the read-out of the reservoir state $t_* \geq \tau$, we yield the output of the reservoir network weighted by a set of tunable output weights $\{W_j^{out}\}$ in appropriate basis. Since we know the labels for the states in the training set (1-entangled, 0-separable), we can optimize the set of weights $\{W_j^{out}\}$ by linear regression, providing the best output for a given training set.

In our simulations, we used two different schemes for the preparation of learning samples. The first method was to use two separate qubits, prepared in either a product or an entangled state, and coupled to the reservoir by Hamiltonian (9). In this method, the teacher states were two-qubit states, which were either entangled or separable states. In the second method, described in [31], the training set was constructed from the two-mode squeezed thermal states described in the Fock basis.

A. Classification of two-qubit states

For classification of two-qubit states, we used the standard $\{0, 1\}$ qubit basis. The teacher states were given by 4×4 density matrices ρ^{teach} defined as follows:

Product states: with density matrices generated as a direct product of two one-qubit states

$$\rho_{separ}^{teach} = |i\rangle \rho_{ij}^1 \langle j| \otimes |k\rangle \rho_{kl}^2 \langle l|$$

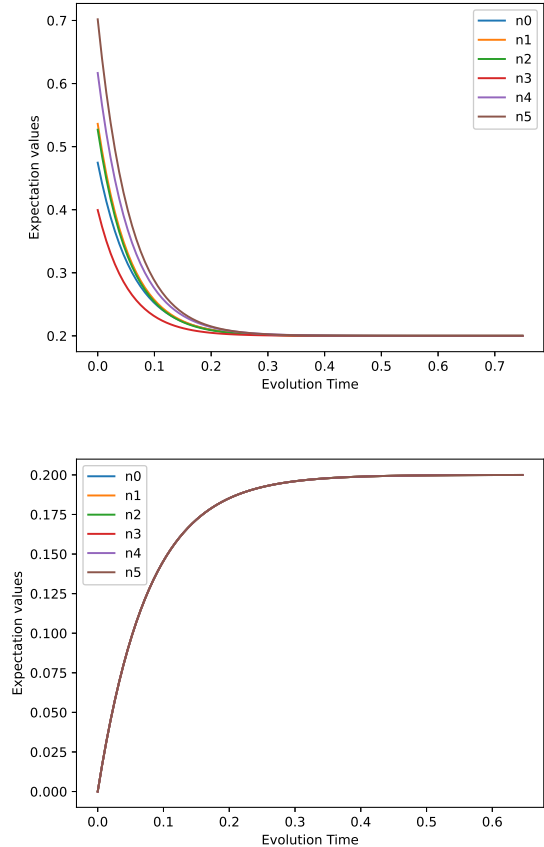


FIG. 2. Equilibration of ground state of 6 qubit reservoir by Lindblad evolution. In the bottom and top pictures we plot the mean populations $n_i = b_i^\dagger b_i$ for the evolution from a random product state of 6 qubits (top), and from the common ground state (bottom), respectively. In the latter case all populations behave identically. Following [31], time t is measured in units of inverse spectral radius of the reservoir Hamiltonian (8), determined by a set of random coefficients J_{ij} .

Entangled states: General 4×4 Hermitian matrices ρ^{teach} with unit trace, constrained from below by the threshold minimal value of log-negativity [$\nu_{min} = 0.15$ in our simulations].

The learning process was organized as follows. Having set the random input weights $W_j, j = \overline{0,5}$ and the reservoir Hamiltonian couplings $J_{i,j}, i, j = \overline{0,5}$ parameters, the state of six-qubit reservoir was equilibrated according to the master equation (10) during the time $T_{equilibration}$. In the learning cycle, we sequentially generate random two-qubit teacher states, as defined above, and connect them to reservoir qubits by the Hamiltonian (9) during the time $T_{reading}$.

The process of mutual evolution of the total $6 + 2$ qubit system ('reading' process) was implemented by the Lindblad-Gorini-Kossakowski-Sudarshan master equation (10) using standard *qutip Python library* for

open quantum system simulations [33].

The novelty of our approach (if compared to [31]) is the reading of 5d output performed by taking the expectation values of five projectors onto 5 singlet states appearing in the direct product of six qubit states [20]

$$P_I = |I\rangle\langle I|. \quad (11)$$

These expectation values are given by the traces of the convolution of projection operators with the reservoir density matrix $\rho^{reservoir}$. For technical reasons the numerical simulation was accomplished in 8 qubit basis with the total density matrix ρ , followed by tracing over the states of teacher qubits ($i = 6, 7$), so that

$$m_I = \text{Tr}(\rho P_I). \quad (12)$$

Five expectation values m_I were fed to the linear regression

$$\sum_{I=1}^5 W_I^{out} m_I(X) = Y(X), \quad (13)$$

where $Y(X) \in \{0, 1\}$ is the label of the class for the element X of the training set. Linear regression was provided by *sklearn Python library* [34].

A typical Lindblad evolution of five singlet expectation values (12) during the 'reading' process is shown in Fig. 3, for entangled (top) and the product (bottom) teacher states, respectively. The parameters used in our simulations of the learning process were

$$\begin{aligned} \gamma &= \max |\text{Eigenvalues}(H_R)|, P = 0.5\gamma \\ T_{equilibration} &= 0.2\gamma, T_{reading} = 0.01\gamma, \end{aligned} \quad (14)$$

that is all time intervals were measured in the units of the inverse spectral radius of Hamiltonian H_R . The teachers' coupling constants were set to big values, $f_k = 10.0$, providing the strong entanglement process between the teacher and the reservoir qubits.

The results of tests of the trained network on the training set of 10 random two-qubit samples are presented in Fig. 4. We compare the performance of our singlet-based reservoir network with that of a quantum reservoir network which uses mean populations $\langle n_i \rangle = \langle b_i^\dagger b_i \rangle$ of all six qubits $i = \overline{0,5}$ for the output [31]. As it can be seen from Fig. 4, the performance of such reservoir network is rather modest for either of the cases: (S) our singlet basis or (N) population basis. The relative recognition error is at best in $\epsilon \in [0.2, 0.3]$ for a small number of training samples in a range of few hundreds of samples. Training sets of larger size drive reservoir networks to over-learning events. The reason for such performance is a relatively small number of degrees of freedom of two-qubit teachers that are imprinted in the reservoir dynamics during the 'reading' process.

In the next section, we have significantly improved the performance of reservoir learning by choosing two-mode squeezed thermal states as a training set, as was implemented in [31]. Even for a small dimension of the

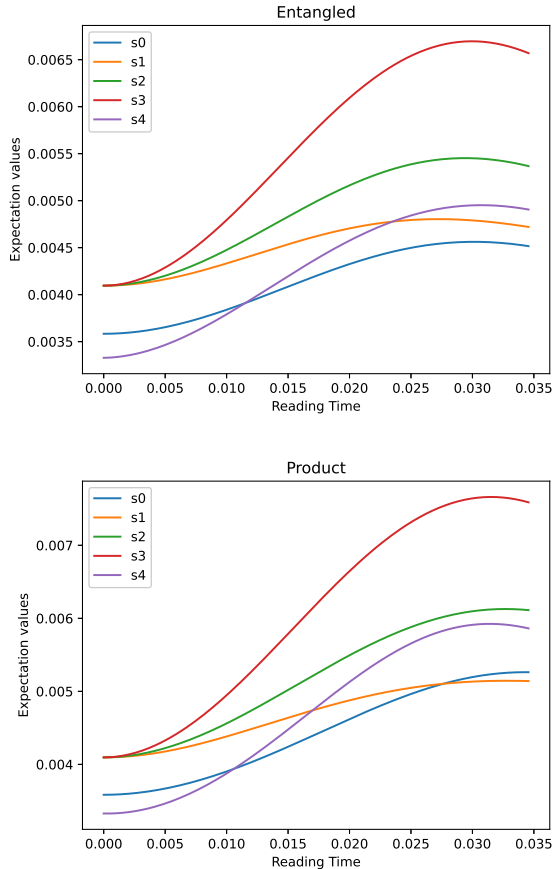


FIG. 3. Typical Lindblad evolution of 5 singlet expectation values m_0, \dots, m_4 during the 'reading' process by interaction of 6 qubit reservoir with 2 teacher qubits. The evolution is shown for an entangled teacher state (top), and product teacher state (bottom).

Fock state, $N_F = 4$, the teacher state density matrix for squeezed states becomes 16×16 density matrix (rather than 4×4 density matrix for two-qubit states). This makes the learning process essentially more effective.

B. Classification of two-mode squeezed states

In the second method, following [31], we used two-mode Fock basis, with maximal mode occupation number $N_F - 1 = 3$. This gives 16×16 density matrix ρ^{teach} for the input states. In the case of *product states* this matrix is generated as a direct product of two independent 4×4 density matrices, of the first and second mode, respectively. For the *entangled states* the density matrix is generated by means of squeezing of thermal states.

The mean occupation number of a boson mode in the thermal state is defined as

$$\bar{n} = \frac{1}{Z(\beta)} \sum_{n=0}^{\infty} n e^{-\beta n}, \quad Z(\beta) = \sum_{n=0}^{\infty} e^{-\beta n}, \quad (15)$$

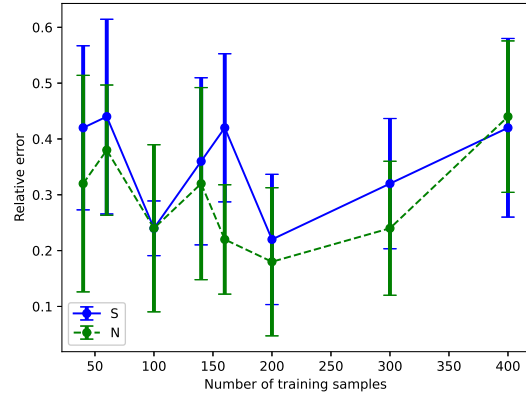


FIG. 4. Comparison of reservoir learning processes performed in our 5 singlet basis (S) and that performed in 6 population basis (N) according to [31]

which gives

$$\bar{n} = \frac{1}{e^{\beta} - 1}, \quad \beta = \ln \left(1 + \frac{1}{\bar{n}} \right). \quad (16)$$

If the total occupation number is restricted by the maximal occupation number $N_F - 1$, the probability of having n_1 quanta in the first mode and n_2 quanta in the second mode, is given by

$$\rho_{n_1, n_2} = \frac{e^{-\beta(n_1+n_2)}}{Z_1^2(\beta)}, \quad Z_1(\beta) = \sum_{j=0}^{N_F-1} e^{-\beta j}. \quad (17)$$

The latter equation is symmetric with respect to the first and second modes and depends on the sum of populations only. The density matrix of a totally mixed thermal state is

$$\hat{\rho}_{th} = \sum_{n_1, n_2=0}^{N_F-1} |n_1, n_2\rangle \rho_{n_1, n_2} \langle n_1, n_2|. \quad (18)$$

The action of annihilation and creation operators (of each mode) in the Fock basis are determined as

$$a|n\rangle = \sqrt{n}|n-1\rangle, \quad a^\dagger|n\rangle = \sqrt{n+1}|n+1\rangle.$$

So, that for $N_F = 4$ the single-mode annihilation operator is given by 4×4 matrix

$$a = \begin{pmatrix} 0 & \sqrt{1} & 0 & 0 \\ 0 & 0 & \sqrt{2} & 0 \\ 0 & 0 & 0 & \sqrt{3} \\ 0 & 0 & 0 & 0 \end{pmatrix}.$$

For the two-mode system, described by 16×16 density matrix in $|n_1, n_2\rangle$ Fock basis, there are two annihilation operators

$$A_1 = a \otimes \mathbb{I}, \quad A_2 = \mathbb{I} \otimes a, \quad (19)$$

for the first and the second mode, respectively, and two creation operators A_1^\dagger, A_2^\dagger . If the modes are independent, the ladder operators of different modes commute to each other.

The correlated state can be obtained from a thermal two-mode state (18) by applying *squeezing* operator

$$S = \exp\left(\alpha A_1^\dagger A_2^\dagger - \bar{\alpha} A_1 A_2\right), \quad (20)$$

where α is arbitrary complex number, and $\bar{\alpha}$ denotes its complex conjugation.

For arbitrary complex number α , applying operator S , we can map a mixed thermal state (18) into a squeezed state

$$\hat{\rho}_{th} \rightarrow v = S \hat{\rho}_{th} S^\dagger. \quad (21)$$

For the simulation of squeezed states v we went along the lines of the work [31]. To do so we used random parameters uniformly distributed in the domains

$$\phi \in \left[\frac{1}{2} - \frac{\pi}{10}, \frac{1}{2} + \frac{\pi}{10}\right], s \in [0.8, 0.95], \theta \in [0, 2\pi]. \quad (22)$$

With these parameters we have defined the mean occupation number of two modes \bar{n} and the inverse temperature β as

$$\bar{n} = s^2 \cos^2 \phi, \quad \beta = \ln\left(1 + \frac{1}{\bar{n}}\right). \quad (23)$$

Having defined the inverse temperature β , we construct $N_F^2 \times N_F^2$ diagonal density matrix for thermal states defined by probabilities (17):

$$\rho_{n_1 n_2, n_1 n_2}^{thermal} = \text{diag} \frac{e^{-\beta(n_1 + n_2)}}{Z_1^2}. \quad (24)$$

To generate entangled two-mode states, we squeeze thermal states (24) with squeezing parameters uniformly distributed in the domain (22). Namely, the complex squeezing parameter is given by

$$\alpha = s \sin(\phi) e^{i\theta}, \quad (25)$$

so that squeezing operator is given by (20,21). For each random sample of parameters for the squeezed state v we calculated the logarithmic negativity to estimate how much the state is entangled. In our simulation we chose a threshold $\nu_{min} = 0.15$, above which we consider the simulated state v as entangled. The logarithmic negativity is calculated in a usual way [35, 36]. We take the matrix G , which is a partial transpose of matrix v with respect to the indices of the second mode. The logarithmic negativity is then given by

$$\text{logneg}(v) = \log_2 \text{Tr}(GG^\dagger). \quad (26)$$

We taught the reservoir network by even number of samples, where each odd sample was a product state

given by a direct product of two $N_F \times N_F$ random density matrices, and each even sample taken as a squeezed state (21), with a log-negativity exceeding the threshold value ν_{min} . In the simulation with Fock state density matrices we used the same set of evolution parameters (14) and coupling constants as for two-qubit teacher simulations. However, since the density matrix for two-mode system with $N = 4$ is 16 times larger than that for two-qubit system, the learning process turns to be more effective.

As we have observed, the learning process effectively starts from a 4 sample set, which contains only two entangled and two product states of two modes in Fock basis, see Fig. 5. Starting from the training sets of approximately 12 learning samples, the recognition on a 12 sample test set becomes almost ideal: no errors were observed during 5 runs on the same volume set. We have

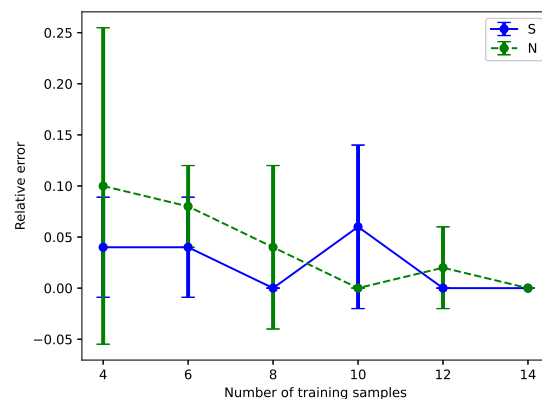


FIG. 5. Comparison of the relative classification errors measured on a 10 sample test set for quantum reservoir learning for different volumes of the training set. The graphs are shown for singlet-based network (S) and the population-based network (N).

observed recognition errors on the 10 sample test set only when the volume of the training set was less than 14; otherwise, all 10 samples received correct recognition during at least 5 runs. We were not able to observe any over-learning effects for the training set volume below 3000 samples.

V. CONCLUSION

Classical reservoir networks have emerged from recurrent neural networks as an effective tool for the analysis of time-dependent data. This method is believed to mimic in some way the operations of biological brain [30]. Quantum reservoir networks are of their own interest for classification of quantum data. They are also considered as alternative to quantum state tomography [37].

In this paper, we consider quantum reservoir networks from the standpoint whether at certain conditions they can perform quantum information processing at ambient

temperature, without a special cooling system as that demanded by common quantum computers. The presented mathematical toy-model harnesses the reading of quantum reservoir state by means of its projections onto decoherence-free subspace. These projections are not affected by large-scale environmental fluctuations.

Same as originally proposed by Zanardi and Rasetti [20], we do not have any explicit mechanism for reading of singlet states amplitudes, and this remains an open question. However, in theoretical model the amplitudes can survive under environmental fluctuations, so a reservoir network with an output in DFS can be considered as a prototype (proof-of-principle) of a room-temperature

quantum information processing system.

On the other hand, since the classification of quantum states into entangled and separable states is of great practical importance for quantum communication and quantum information processing, we can also think of *in silico* implementation of such quantum reservoir networks, complementary to the known optical reservoir processing [29, 37].

ACKNOWLEDGEMENT

The authors are thankful to Profs. L.Fedichkin and R.Nazmitdinov for useful comments.

-
- [1] B.M. Lake, T.D. Ullman, J.B. Tenenbaum, and S.J. Gershman, “Building machines that learn and think like people,” *Behavioral and Brain Sciences* **40**, e253 (2017).
- [2] D. Deutsch, “Quantum theory, the Church-Turing principle and the universal quantum computer,” *Proc. Roy. Soc. Lond.* **A400**, 97–117 (1985).
- [3] P. Shor, “Polynomial-time algorithm for prime factorization and discrete logarithms on a quantum computer,” in *Proceedings of 35th Annual Symposium on Foundations of Computer Science* (IEEE Press, Piscataway, NJ, 1994).
- [4] L.K. Grover, “Quantum mechanics helps in searching for a needle in a haystack,” *Phys. Rev. Lett.* **79**, 325–328 (1997).
- [5] H.D. Zeh, “On the interpretation of measurement in quantum theory,” *Foundations of Physics* **1**, 69–76 (1979).
- [6] D. Giulini, E. Joos, C. Kiefer, J. Kupsch, I.-O. Stamatescu, and H.-D. Zeh, *Decoherence and the appearance of classical world in quantum theory* (Springer-Verlag, NY/Berlin, 1996).
- [7] P. W. Shor, “Scheme for reducing decoherence in quantum computer memory,” *Phys. Rev. A* **52**, R2493–R2496 (1995).
- [8] A. Steane, “Multiple-particle interference and quantum error correction,” *Proceedings of the Royal Society A: Mathematical, Physical and Engineering Sciences* **452**, 2551–2577 (1996).
- [9] R. Feynman, “Simulating physics with computers,” *Int. J. Theor. Phys.* **21**, 467–488 (1982).
- [10] D.C. Hebb, *Organization of behavior* (Wiley, NY, 1949).
- [11] S. Haykin, *Neural Networks and Learning Machines* (Pearson Education, 2009).
- [12] Y. LeCun, Y. Bengio, and G. Hinton, “Deep learning,” *Nature* **521**, 436–444 (2015).
- [13] V. Chavchanidze, “On spatial-temporal quantum-wave processes in neural networks,” *Soobshch. AN Gruzinskoi SSR* **59**, 37–40 (1970).
- [14] F. Beck and J. Eccles, “Quantum aspects of brain activity and the role of consciousness,” *PNAS* **89**, 11357–11361 (1992).
- [15] S. Hagan, S. R. Hameroff, and J. A. Tuszynski, “Quantum computation in brain microtubules: Decoherence and biological feasibility,” *Phys. Rev. E* **65**, 061901 (2002).
- [16] B. Adams and F. Petruccione, “Quantum effects in brain: A review,” *AVS Quantum Science* **2**, 022901 (2020).
- [17] P. Kurian, “Computational capacity of life in relation to the universe,” *Sci. Adv.* **11**, eadt4623 (2025).
- [18] M. Tegmark, “Importance of quantum decoherence in brain processes,” *Phys. Rev. E* **61**, 4194–4206 (2000).
- [19] E. Collini, C.Y. Wong, K.E. Wilk, P.M.G. Curmi, P. Brumer, and G.D. Scholes, “Coherently wired light-harvesting in photosynthetic marine algae at ambient temperature,” *Nature* **463**, 644–647 (2010).
- [20] P. Zanardi and M. Rasetti, “Noiseless quantum codes,” *Phys. Rev. Lett.* **79**, 3306–3309 (1997).
- [21] D.A. Lidar, I.L. Chuang, and K.B. Whaley, “Decoherence-free subspaces for quantum computation,” *Phys. Rev. Lett.* **81**, 2594–2597 (1998).
- [22] M. Altaisky and N. Kaputkina, “Towards a room-temperature quantum reservoir computing,” *J. Innovation Sciences and Sustainable Technologies* **5**, 83–93 (2025).
- [23] H.P. Breuer and F. Petruccione, *The theory of open quantum systems* (Oxford University Press, 2002).
- [24] G.M. Palma, K.-A. Suominen, and A.K. Ekkert, “Quantum computers and dissipation,” *Proc. R. Soc. Lond. A* **452**, 567–584 (1996).
- [25] A.J. Leggett, S. Chakravarty, A.T. Dorsey, M.P.A. Fisher, A. Garg, and W. Zwerger, “Dynamics of the dissipative two-state system,” *Rev. Mod. Phys.* **59**, 1–85 (1987).
- [26] K. Hepp and E. H. Lieb, “Equilibrium statistical mechanics of matter interacting with the quantized radiation field,” *Phys. Rev. A* **8**, 2517–2525 (1973).
- [27] J.F. Cornwell, *Group theory: An Introduction* (Academic Press Limited, 1997).
- [28] Johnson M. W., Amin M. H. S., Gildert S., Lanting T., Hamze F., Dickson N., Harris R., Berkley A. J., Johanson J., Bunyk P., Chapple E. M., Enderud C., Hilton J. P., Karimi K., Ladizinsky E., Ladizinsky N., Oh T., Perminov I., Rich C., Thom M. C., Tolkacheva E., Truncik C. J. S., Uchaikin S., Wang J., Wilson B., and Rose G., “Quantum annealing with manufactured spins,” *Nature* **473**, 194–198 (2011).
- [29] Y. Paquot, F. Duport, A. Smerieri, J. Dambre, B. Schrauwen, M. Haelterman, and S. Massar, “Opto-

- electronic reservoir computing,” *Sci. Rep.* **2**, 287 (2012).
- [30] L. Larger, A. Baylón-Fuentes, R. Martinenghi, V.S. Udaltsov, Y. K. Chembo, and M. Jacquot, “High-speed photonic reservoir computing using a time-delay-based architecture: Million words per second classification,” *Phys. Rev. X* **7**, 011015 (2017).
- [31] S. Ghosh, A. Opala, M. Matuszewski, T. Paterek, and T.C.H. Liew, “Quantum reservoir processing,” *npj Quantum Inf.* **5**, 35 (2019).
- [32] M. Altaisky and N. Kaputkina, “Quantum reservoir computing based on decoherence-free subspaces,” in *2025 Days on Diffraction (DD)* (IEEE, St.Petersburg, 2025) pp. 6–12.
- [33] N. Lambert, E. Giguère, P. Menczel, B. Li, P. Hopf, G. Suárez, M. Gali, J. Lishman, R. Gadhvi, R. Agarwal, A. Galicia, N. Shammah, P. Nation, J. R. Johansson, S. Ahmed, S. Cross, A. Pitchford, and F. Nori, “Qutip 5: The quantum toolbox in Python,” *Physics Reports* **1153**, 1–62 (2026).
- [34] F. Pedregosa and a.o., “Scikit-learn: Machine learning in Python,” *Journal of Machine Learning Research* **12**, 2825–2830 (2011).
- [35] V. Vidal and R.F. Werner, “Computable measure of entanglement,” *Phys. Rev. A* **65**, 032314 (2002).
- [36] M. B. Plenio, “Logarithmic negativity: A full entanglement monotone that is not convex,” *Phys. Rev. Lett.* **95**, 090503 (2005).
- [37] D. Zia, L. Innocenti, G. Minati, S. Lorenzo, A. Suprano, R. Di Bartolo, N. Spagnolo, T. Giordani, V. Cimini, G.M. Palma, A. Ferraro, F. Sciarrino, and M. Paternostro, “Quantum reservoir computing for photonic entanglement witnessing,” *Science Advances* **11**, ady7987 (2025).